Gear Surface Roughness Induced Noise Prediction Based on a Linear Time-varying Model with Sliding Friction

SEUNGBO KIM
RAJENDRA SINGH
Acoustics and Dynamics Laboratory, Department of Mechanical Engineering and The Center for Automotive Research, The Ohio State University, Columbus, OH 43210, USA
(Email: singh.3@osu.edu)

(Received 20 March 2006; accepted 24 May 2006)

Abstract: This article presents a new gear surface roughness induced noise source model while taking into account the sliding contacts between meshing gear teeth. The surface asperities on tooth surfaces are modeled as compact structural beam elements that radiate sound in the off-line of action after sliding impacts, against asperities of the meshing surface, occur. A linear time-varying (LTV) model of a spur gear pair (with sliding friction) is employed to calculate the instantaneous sliding velocity between pinion and gear teeth, which is then applied to the asperities as the initial condition. The transient sound field from the flexural motions of surface asperities (acoustically baffled along their axes), which are released from the cylindrical Hertzian contact zone in gear teeth, is computed. The modal superposition method is used for far and free field calculations given the surface roughness and its (assumed) asperity distribution on the tooth profile. Typical sound pressure predictions show that the noise levels increase with operating speeds and surface roughness.

Key words: Gear dynamics, acoustic source, surface roughness, sliding friction

1. INTRODUCTION

Steady state gear (whine) noise is typically generated by several sources but the static transmission error is the most commonly analyzed excitation (Houser, 1991; Houser and Singh, 2001). For this problem, the structure-borne noise path (through the gear-shaft-bearing-casing system) is the dominant one as the noise is often radiated by the casing and surrounding structures. Mechanisms associated with other gear noise sources including the surface roughness and sliding friction have not been adequately analyzed. In particular, Mitchell (1971) presented experimental results that show that gear noise increases with surface roughness and operating speed. Ishida and Matsuda (1980) examined the effect of tooth surface roughness on gear noise based on the structural vibration of gear system. Further, Mark (1992) analytically investigated the effects of gear tooth surface periodicity on vibratory behavior of a geared system excited by the transmission error. The air-borne noise source, di-

Journal of Vibration and Control, **13(7):** 1045–1063, 2007 DOI: 10.1177/1077546307078829

Figures 1, 3–11 appear in color online: http://jvc.sagepub.com

rectly from gear teeth surfaces, has rarely been investigated though some attempts have been made to study the aerodynamic sources (Houjou and Umezawa, 1992; Jacobson et al., 1996) and radiation from the casing using ideal acoustic sources. The air-borne noise source should become particularly important in those high speed operations where the gear profiles have already been optimized for minimal static transmission error. No theoretical model that could explain the surface roughness induced noise generation mechanism is currently available. Therefore, in this article, we present a new airborne noise source model that is generated by the sliding contacts between surface asperities on the gear teeth. Given the complexity of this problem, some idealized conditions must be employed such as acoustically baffled boundaries along their asperity axes in the free far-field. As a consequence, sound interactions among the asperity elements will be beyond the scope of the present work. Further, a linear time-varying (LTV) formulation with sliding friction will be utilized to model the spur gear pair.

The role of sliding friction leading to time-varying models and non-linearities is the subject of recent investigations (Vaishya and Singh, 2001; Vaishya and Singh, 2003). However, those analyses have focused on the gear dynamic behavior and not on the noise source. In earlier work, Aziz and Seireg (1994) conducted a parametric study of the gear frictional noise by defining an empirical relative noise level, which was defined as the ratio of sound pressure in a lubricated regime to that in the dry regime. This idea deals with the condition that the surface penetration reaches the average surface roughness and assumes a simple proportional relationship between the sound generation and the surface penetration. However, the underlying theoretical linkage between surface contact and noise generation was not established and thus its applicability is very limited. Overall, the nature of the frictional noise is yet to be understood because of the complexity in modeling the surface details and lubrication regimes. Accordingly, some researchers have used generic solid surfaces to formulate the problem. For instance, Baranov et al. (1997) correlated the emitted acoustic energy with contact zone deformation and described an empirical friction-induced noise level. The statistical distribution of noise from friction surface was calculated by using statistically populated surface asperities. However, such an energy relation lacks physical interpretation. In yet another prior study, Othman et al. (1990) established a relation between the sound pressure and surface roughness given experimental data of surface friction in a rotating disk. Again, the general applicability of such relationship(s) is questionable. Finally, Akay (2002) has reviewed friction-induced vibration and acoustics for a broad range of mechanical systems (but not the gears). Overall, it is evident that the gear friction and roughness-induced noise sources have to be properly investigated.

2. PROBLEM FORMULATION

Chief objectives of this study include: 1. Develop a specific air-borne noise generation in terms of the sliding contacts between meshing gear teeth. 2. Examine the effects of surface roughness and operating speed on surface finish-induced airborne noise. A linear time-varying (LTV) model of a spur gear pair, based on the prior work of Vaishya and Singh (2001, 2003), is employed to describe the dynamic behavior of the gear system and to analyze the surface roughness-induced noise. This model assumes that the tooth surface profiles are known, say through measurements.

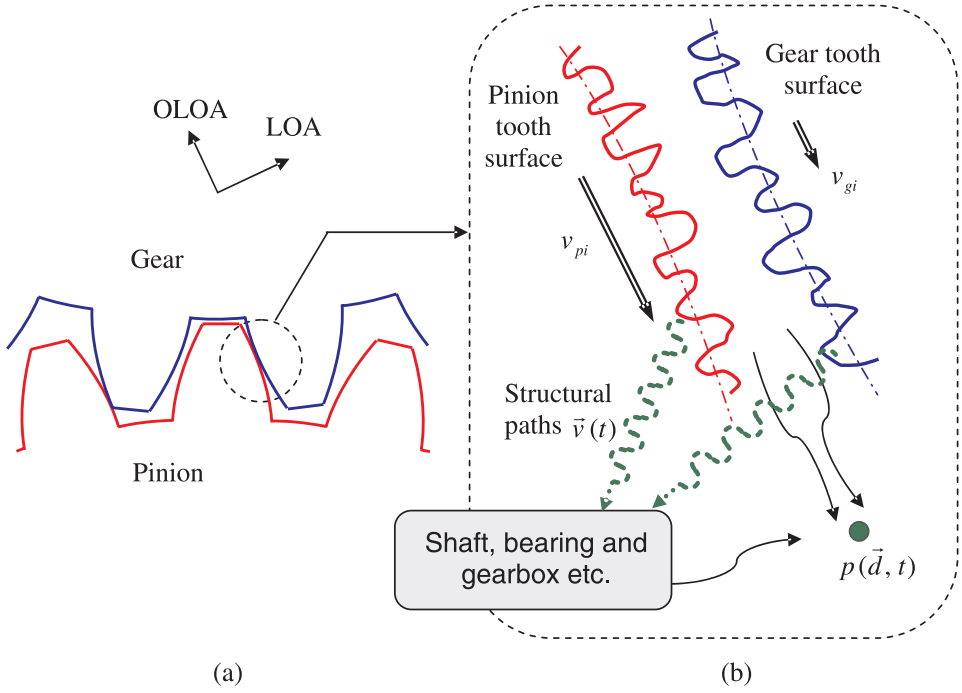

Figure 1. Problem formulation. (a) Spur gear pair in mesh with given surface roughness; (b) related air-borne and structure-borne noise generation. Here, velocity magnitudes (v_{pi} and v_{gi}) of gear tooth surfaces in the sliding direction are depicted by the length of arrows. Further, the undulated surface-induced vibration transmitted to the surrounding structures is denoted by $\vec{v}(t)$. Key: LOA = line of action; OLOA = off-line of action.

The research problem is conceptually shown in Figure 1**,** with emphasis on the air-borne noise, as excited by the surface finish. First, the surface asperities on tooth surfaces are modeled as very small structural beam elements (of very high natural frequencies) that radiate directly sound in the off-line of action after sliding impacts, against asperities of the meshing part, occur. These asperities are assumed to remain in the elastic regime during the meshing cycles. The transient sound field from the flexural motions of surface asperities, which are released from the cylindrical Hertzian contact zone in gear teeth, is calculated given the surface roughness and its (assumed) probabilistic population on the tooth profile. The instantaneous sliding velocity between pinion and gear teeth (from the previous cycle) is applied to the asperities as initial conditions. Then the modal superposition method is adopted to describe the temporal behavior of asperity structures and the resulting sound radiation. It is assumed that the asperities are acoustically baffled along their axes (normal to the gear tooth surface) for the prediction of far-field sound. Further, only the free field is considered here and thus sound interactions among the asperity elements are not included in our model.

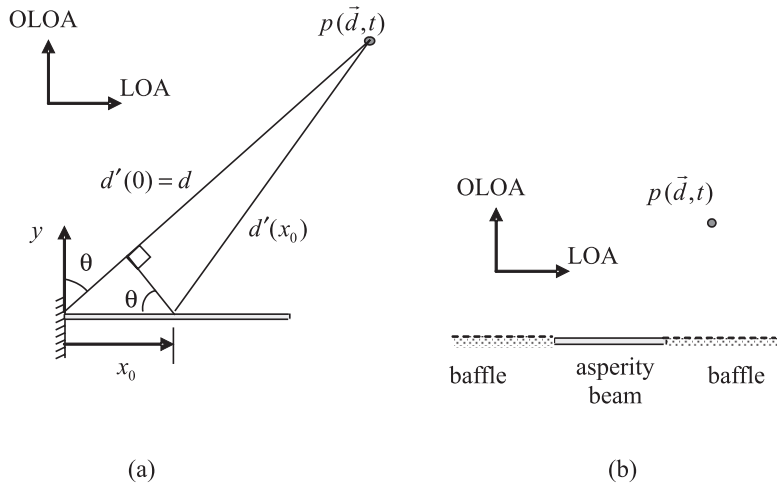

Figure 2. Sound radiation from an asperity modeled as a cantilever beam (clamped to the gear tooth surface). (a) Schematic for sound radiation calculation. (b) Baffle configuration.

3. TRANSIENT SOUND RADIATED FROM AN ASPERITY BEAM

Consider an asperity beam on the gear tooth surface, as shown in Figure 2(a) along with the gear contact coordinates which are denoted by the Line of Action (LOA) and Off-Line of Action (OLOA). The cantilever beam of Figure 2(a), describing an asperity, is fixed to the gear tooth surface. It is assumed to be acoustically baffled, along the LOA that is normal to the gear tooth surface as illustrated in Figure 2(b). This baffle assumption is made to develop a tractable problem though it somewhat deviates from reality. The acoustic wave equation with sources distributed over the cantilever beam is as follows where Φ and ∇ are the velocity potential and Laplace operator respectively:

$$\frac{\partial^2 \Phi(x,t)}{\partial t^2} - \nabla^2 \Phi(x,t) = v(\vec{x}_0, t_0) b dx_0. \tag{1}$$

Here, $v(\vec{x}_0, t_0)$ is the velocity distribution over the asperity beam with the width b and acoustic field is considered in the half space where $y \geq 0$. Refer to Appendix A for the identification of symbols. The solution to the wave equation is expressed as follows where $g(\vec{x}, t \mid \vec{x}_0, t_0)$ is the Green's function when the beam is acoustically baffled and $\delta(\cdot)$ is the Dirac Delta function (Stepanishen, 1971):

$$\Phi(x,t) = \int_0^t \int_0^l \left[v(\vec{x}_0, t_0) \cdot g(\vec{x}, t | \vec{x}_0, t_0) \cdot b \right] dx_0 dt_0, \tag{2a}$$

$$g(\vec{x}, t | \vec{x}_0, t_0) = \frac{\delta(t - t_0 - \left| \vec{x} - \vec{x}_0 \right| / c)}{2\pi \left| \vec{x} - \vec{x}_0 \right|}. \tag{2b}$$

By taking an integral over t_0, the velocity potential is written as

$$\Phi(x,t) = \frac{b}{2\pi}\int_0^l \frac{v(\vec{x}_0,\ t - \left|\vec{x} - \vec{x}_0\right|/c)}{\left|\vec{x} - \vec{x}_0\right|}\, dx_0. \tag{3}$$

Further, the sound pressure is expressed as

$$p(x,t) = \rho\frac{\partial\Phi(x,t)}{\partial t} = \frac{\rho b}{2\pi}\int_0^l \frac{\partial}{\partial t}\left[\frac{v(\vec{x}_0,\ t - \left|\vec{x} - \vec{x}_0\right|/c)}{\left|\vec{x} - \vec{x}_0\right|}\right] dx_0. \tag{4}$$

By substituting $x - x_0 = d'(x_0)$ into (4), the sound pressure is represented as

$$p(x,t) = \frac{\rho b}{2\pi d}\int_0^l \frac{\partial v\,(x_0,\ t - d'(x_0)/c)}{\partial t}\, dx_0, \tag{5a}$$

$$d'(x_0) \approx d - x_0\sin\theta. \tag{5b}$$

Here, the approximation $x - x_0 \approx d$ has been used for the denominator; it usually adopted for the harmonic case (Singh and Kim, 2003). Next, the velocity distribution of a clamped-free beam is obtained via the modal superposition method. Given the initial conditions $y(x,0)$ and $\dot{y}(x,0)$, the homogeneous governing equation of the beam (in flexure) is

$$EI\frac{\partial^4 y(x,t)}{\partial x^4} + \rho S\frac{\partial^2 y(x,t)}{\partial t^2} = 0. \tag{6}$$

The transverse displacement (y) of the beam is expressed as follows where $\phi_r(x)$ and $q_r(t)$ are the rth normal mode and the free vibration of the normal mode respectively (Timoshenko, 1974):

$$y(x,t) = \sum_{r=1}^{\infty}\frac{\phi_r(x)}{N_r}q_r(t), \quad N_r = \int_0^L \phi_r^2(x)dx. \tag{7a, b}$$

The $\phi_r(x)$ and $q_r(t)$ satisfy the following relations:

$$\frac{d^4\phi_r(x)}{dx^4} - \kappa^4\phi_r(x) = 0, \quad \frac{\partial^2 q_r(t)}{\partial t^2} + 2\xi\omega_r\frac{\partial q_r(t)}{\partial t} + \omega_r^2 q_r(t) = 0. \tag{8a, b}$$

Substituting $y(x,0)$ and $\dot{y}(x,0)$ into the following relations, the initial conditions of $q_r(t)$ in the normal mode coordinates are obtained as follows:

$$q_r(0) = \int_0^L y(x,0)\phi_r(x)dx, \quad \dot{q}_r(0) = \int_0^L \dot{y}(x,0)\phi_r(x)dx. \tag{9a, b}$$

Solving (8b) with $q_r(0)$ and $\dot{q}_r(0)$ yields the following:

$$q_r(t) = \exp(-\sigma_r t)\left[q_r(0)\cos(\omega_{dr}t) + \frac{[\sigma_r q_r(0) + \dot{q}_r(0)]}{\omega_{dr}}\sin(\omega_{dr}t)\right]. \tag{10}$$

The eigenfunction (mode) of the clamped-free beam is well known as:

$$\phi_r(x) = \cosh(\kappa_r x) - \cos(\kappa_r x) - \varepsilon_r[\sinh(\kappa_r x) - \sin(\kappa_r x)], \tag{11a}$$

$$\varepsilon_r = \frac{\sinh(\kappa_r L) - \sin(\kappa_r L)}{\cosh(\kappa_r L) - \cos(\kappa_r L)}. \tag{11b}$$

The $\phi_r(x)$ of the beam is normalized as

$$\int_0^L \phi_i(x)\phi_j(x)dx = \begin{cases} 0 & \text{for} \quad i \neq j \\ L & \text{for} \quad i = j \end{cases}. \tag{12}$$

In this article, the following initial conditions are employed to describe the asperity impact during the sliding motions of gear teeth where δ and v_{S0} represent the portion of beam under impact and sliding velocity respectively.

$$y(x,0) = 0, \quad \dot{y}(x,0) = \begin{cases} 0 & \text{for} \quad 0 \le x < L - \delta \\ v_{S0} & \text{for} \quad L - \delta \le x < L \end{cases}. \tag{13a, b}$$

By using the relation (9), the above initial conditions are converted to the modal coordinates as follows:

$$q_r(0) = 0, \quad \dot{q}_r(0) = \int_{L-\delta}^{L}[v_{S0}\phi_r(x)]dx = \frac{v_{S0}}{\kappa_r}Q_r, \tag{14a, b}$$

$$Q_r = \{\varepsilon_r[\cosh(\kappa_r(L-\delta)) + \cos(\kappa_r(L-\delta))] - \sinh(\kappa_r(L-\delta)) + \sin(\kappa_r(L-\delta))\}. \tag{14c}$$

By applying $q_r(0)$ and $\dot{q}_r(0)$ to equation (10), the free vibration of each mode is obtained as:

$$q_r(t) = \frac{v_{S0}Q_r}{\omega_{dr}\kappa_r}\exp(-\sigma_r t)\sin(\omega_{dr}t). \tag{15}$$

The displacement and velocity distributions of the beam are obtained respectively as:

$$y(x,t) = \sum_{r=1}^{\infty}\frac{\phi_r(x)v_{S0}Q_r}{\omega_{dr}(\kappa_r L)}\exp(-\sigma_r t)\sin(\omega_{dr}t). \tag{16a}$$

$$\dot{y}(x,t) = \sum_{r=1}^{\infty}\frac{\phi_r(x)v_{S0}Q_r}{\omega_{dr}(\kappa_r L)}\exp(-\sigma_r t)\left[-\sigma_r\sin(\omega_{dr}t) + \omega_{dr}\cos(\omega_{dr}t)\right]. \tag{16b}$$

For convenience, the above velocity distributions are expressed as follows where the superscript * denotes the complex conjugation:

$$\dot{y}(x,t) = \sum_{r=1}^{\infty} \frac{\phi_r(x) v_{S0} Q_r}{\omega_{dr}(\kappa_r L)} \frac{[\Lambda_r \exp(\Lambda_r t) - \Lambda_r^* \exp(\Lambda_r^* t)]}{2j}. \tag{17a}$$

$$\Lambda_r = -\sigma_r + j\omega_{dr}, \quad \Lambda_r^* = -\sigma_r - j\omega_{dr}. \tag{17b, c}$$

$$\phi_r(x) = A\exp(\kappa_r x) + B\exp(-\kappa_r x) + C\exp(j\kappa_r x) + D\exp(-j\kappa_r x), \tag{17d}$$

$$A = (1-\varepsilon_r)/2, \quad B = (1+\varepsilon_r)/2, \tag{17e, f}$$

$$C = (-1-j\varepsilon_r)/2, \quad D = (-1+j\varepsilon_r)/2. \tag{17g, h}$$

By applying the velocities of the beam to (5a), the sound pressure is finally derived as:

$$p(x,t) = \frac{\rho b}{2\pi d} \sum_{r=1}^{n} \frac{v_{S0} Q_r}{\omega_{dr}(\kappa_r L)} \left[\frac{\Lambda_r^2 \exp[\Lambda_r (t - d/c)]}{2j} G_{r1} - \frac{\Lambda_r^{2*} \exp[\Lambda_r^* (t - d/c)]}{2j} G_{r2} \right], \tag{18a}$$

$$\begin{aligned} G_{r1} = {} & \frac{A\left[\exp\left[(\kappa_r + \Lambda_r \sin(\theta)/c)L\right] - 1\right]}{\kappa_r + \Lambda_r \sin(\theta)/c} \\ & + \frac{B\left[\exp\left[(-\kappa_r + \Lambda_r \sin(\theta)/c)L\right] - 1\right]}{-\kappa_r + \Lambda_r \sin(\theta)/c} \\ & + \frac{C\left[\exp\left[(j\kappa_r + \Lambda_r \sin(\theta)/c)L\right] - 1\right]}{j\kappa_r + \Lambda_r \sin(\theta)/c} \\ & + \frac{B\left[\exp\left[(-j\kappa_r + \Lambda_r \sin(\theta)/c)L\right] - 1\right]}{-j\kappa_r + \Lambda_r \sin(\theta)/c}, \end{aligned} \tag{18b}$$

$$\begin{aligned} G_{r2} = {} & \frac{A\left[\exp\left[(\kappa_r + \Lambda_r^* \sin(\theta)/c)L\right] - 1\right]}{\kappa_r + \Lambda_r^* \sin(\theta)/c} \\ & + \frac{B\left[\exp\left[(-\kappa_r + \Lambda_r^* \sin(\theta)/c)L\right] - 1\right]}{-\kappa_r + \Lambda_r^* \sin(\theta)/c} \\ & + \frac{C\left[\exp\left[(j\kappa_r + \Lambda_r^* \sin(\theta)/c)L\right] - 1\right]}{j\kappa_r + \Lambda_r^* \sin(\theta)/c} \\ & + \frac{B\left[\exp\left[(-j\kappa_r + \Lambda_r^* \sin(\theta)/c)L\right] - 1\right]}{-j\kappa_r + \Lambda_r^* \sin(\theta)/c}. \end{aligned} \tag{18c}$$

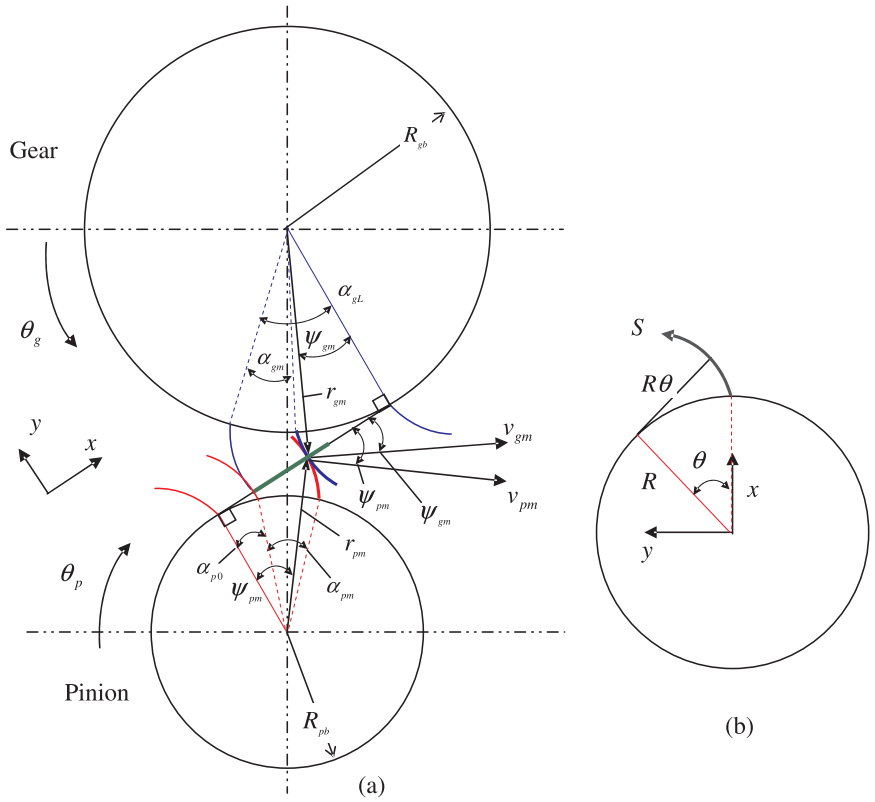

Figure 3. Gear kinematic model. (a) Key roll angles; (b) gear involute coordinate and parameters.

4. KINEMATIC MODEL OF A SPUR GEAR

A meshing spur gear pair is shown in Figure 3 along with key parameters on the gear base circles R_b where α represents the gear roll angle and subscripts p and g denote pinion and gear respectively. Further, subscripts m, 0 and L indicate mesh point, mesh start points of pinion and gear respectively and r is a radial distance to mesh point from the gear centers. The line of action (LOA) and off-line of action (OLOA) are also denoted here by x and y.

The length of gear involute curve with a circle of radius R is known as follows where s is the involute curve coordinate as shown in Figure 3(b):

$$s(\theta) = \int ds = \int \sqrt{(dx/d\theta)^2 + (dy/d\theta)^2}\, d\theta = (1/2)R\theta^2, \tag{19a}$$

$$x = R\cos\theta + R\theta\sin\theta, \quad y = R\sin\theta - R\theta\cos\theta. \tag{19b, c}$$

As the gears roll, the mesh location of pinion and gear at the involute coordinates are:

$$s_p = \frac{1}{2}R_{pb}[\alpha_{p0} + \alpha_{pm}]^2, \quad s_g = \frac{1}{2}R_{gb}[\alpha_{gL} - \alpha_{gm}]^2. \tag{20a, b}$$

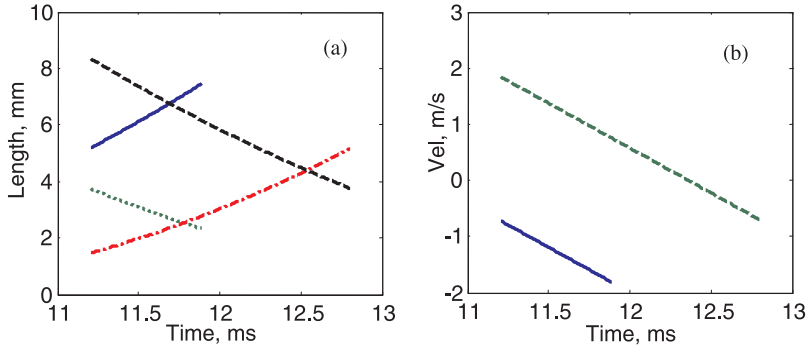

Figure 4. Gear tooth involute parameters for one mesh period given constant operating speeds. (a) Mesh location at involute coordinates. Key: ——, 1st tooth of pinion; ·····, 1st tooth of gear; -·-·-, 2nd tooth of pinion; - - - - 2nd tooth of gear. (b) Sliding speed of meshing teeth in OLOA direction. Key: ——, 1st teeth pair; ·····, 2nd teeth pair.

The radii of involute curvature at the mesh are:

$$\gamma_{pm} = R_{pb}[\alpha_{p0} + \alpha_{pm}], \quad \gamma_{gm} = R_{gb}[\alpha_{gL} - \alpha_{gm}]. \tag{21a, b}$$

The sliding velocity at mesh is expressed as follows where v_{pmx} and v_{gmx} are the velocities of gear and pinion in OLOA direction respectively:

$$v_S = v_{pmx} - v_{pmx}, \tag{22a}$$

$$v_{pmx} = r_{pm}\sin(\psi_{pm})\dot{\theta}_p = R_{pb}[\alpha_{p0} + \alpha_{pm}]\dot{\theta}_p, \tag{22b}$$

$$v_{gmx} = r_{gm}\sin(\psi_{gm})\dot{\theta}_g = R_{gb}[\alpha_{gL} - \alpha_{gm}]\dot{\theta}_g. \tag{22c}$$

Further, the moment arm of the first and second teeth for friction torques are as follows where the subscript c represents mesh cycle:

$$x_{p1m} = R_{pb}[\alpha_{p0} + \alpha_{pc} + \alpha_{pm}], \quad x_{g2m} = R_{gb}[\alpha_{gL} - \alpha_{gc} - \alpha_{gm}], \tag{23a, b}$$

$$x_{p2m} = R_{pb}[\alpha_{p0} + \alpha_{pm}], \quad x_{g2m} = R_{gb}[\alpha_{gL} - \alpha_{gm}]. \tag{23c ,d}$$

Given constant operating speeds, the mesh locations on involute coordinates and sliding velocities of a typical gear pair are shown for one mesh cycle in Figure 4. The mesh locations increase and decrease in a quadratic manner for pinion and gear respectively, as shown in Figure 4(a). Further, Figure 4(b) shows that the sliding direction of the second teeth pair changes at the pitch point.

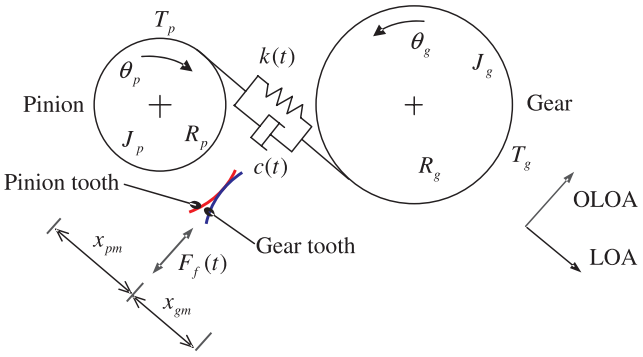

Figure 5. Gear dynamic model with time-varying mesh parameters and sliding friction.

5. LINEAR TIME-VARYING GEAR DYNAMICS MODEL

The linear time-varying (LTV) model with sliding friction, that was developed by Vaishya and Singh (2001, 2003), is employed to describe the dynamic behavior of the gear system. The dynamic model is shown for a spur gear pair in Figure 5 where F_f and x are the sliding friction force and its moment arm respectively. The governing equations are briefly described below:

$$\begin{aligned} & J_p\ddot{\theta}_p + [c(t)(R_p\dot{\theta}_p - R_g\dot{\theta}_g) + k(t)(R_p\theta_p - R_g\theta_g)] \\ \times \quad & [R_p - \sum_i \mu_i(t)x_{pi}(t)] \;=\; T_p, \end{aligned} \tag{24a}$$

$$\begin{aligned} & J_g\ddot{\theta}_g + [c(t)(R_g\dot{\theta}_g - R_p\dot{\theta}_p) + k(t)(R_g\theta_g - R_p\theta_p)] \\ \times \quad & [R_g + \sum_i \mu_i(t)x_{gi}(t)] \;=\; -T_g. \end{aligned} \tag{24b}$$

Here, μ is the friction coefficient and i, j are tooth indices of pinion and gear respectively. The above equations assume rigid shafts and bearings and thus the effects of flexibility of such adjacent structures as shafts, gear casing and bearings are not included in this model. The semi-definite system (24) reduces to the following single degree of freedom model where the dynamic transmission error, Ξ, represents $R_p\theta_p - R_g\theta_g$:

$$\begin{aligned} & J_pJ_g\ddot{\Xi} + [c(t)\dot{\Xi} + k(t)\Xi] \\ \times \quad & \left[J_gR_p^2 + J_pR_g^2 - J_gR_p\sum_i \mu_i(t)x_{pi} - J_pR_g\sum_i \mu_i(t)x_{gi}\right] \\ = \quad & J_gR_pT_p + J_pR_gT_g. \end{aligned} \tag{25}$$

The time-varying parameters of the above equation are chosen as

$$k(t) = \begin{cases} k_1, & 0 \le t < t_s \\ k_2, & t_s \le t < t_c \end{cases}, \quad c(t) = \begin{cases} c_1, & 0 \le t < t_s \\ c_2, & t_s \le t < t_c \end{cases}, \tag{26a, b}$$

$$\mu_1(t) = \begin{cases} -\mu_0, & 0 \le t < t_s \\ 0, & t_s \le t < t_c \end{cases}, \quad \mu_2(t) = \begin{cases} \mu_0, & 0 \le t < t_p \\ -\mu_0, & t_p \le t < t_c \end{cases}. \tag{26c, d}$$

The above LTV model assumes the loads are equally distributed between the pinion and gear via the mesh spring and damping elements and step changes in corresponding mesh stiffness and damping coefficients occur at the mesh transition points. Further, the coefficient of friction changes at the pitch point when the sliding direction reverses but it is assumed that the value of μ remains constant before and after the pitch point. Refer to Vaishya and Singh (2001, 2003) for further details. Furthermore, our model presumes the sliding velocity and mesh locations on teeth that are based on the kinematic relationships of Figure 4. Hence, the effect of vibratory motions on changes in the above parameters is not included in our model.

6. NOISE RADIATED FROM GEAR SURFACE ASPERITIES

Sound generation due to the sliding impacts between gear teeth is schematically shown in Figure 6(a). At a meshing point in the involute coordinates, sliding impacts occur among asperities of the meshing parts within contact zone and these asperities radiate sound in the off-line of action after the sliding impacts. These asperities are assumed to remain in the elastic regime during the meshing cycles. The transient sound field consists of the contributions from only the surface asperities that are released from the contact zone in gear teeth. These asperities are darkly shaded in Figure 6(a). Hence, the sound radiations of asperities inside the contact zone, which are unshaded in Figure 6(a), are not included in the resulting sound field. However, these asperities contribute to the sound field at subsequent impact times. Given a normal force between gear meshing teeth, the width of contact zone is calculated by the cylindrical Hertzian contact model. The contact zone width with the instantaneous radius of curvature γ is obtained as follows, where F_N, b_{Fw}, ν and E represent normal force, face width of gears, Poisson's ratio and Young's modulus respectively (Goldsmith, 2001):

$$z(t) = 4\sqrt{\frac{\gamma_{pm}(t)\gamma_{gm}(t)F_N(t)/b_{Fw}}{\gamma_{pm}(t) + \gamma_{gm}(t)}\left[\frac{1-\nu_p^2}{E_p\pi} + \frac{1-\nu_g^2}{E_g\pi}\right]}. \tag{27}$$

Surface roughness on the gear teeth is described by the averaged quantities such as the asperity height h and distance λ between asperities. Further, the asperity beam width and thickness are denoted here as b and t respectively. These surface roughness descriptions are depicted in Figure 6(b).

The instantaneous sliding velocity between pinion and gear teeth (from the previous cycle) is applied to the asperities over the half of the asperity height as initial conditions.

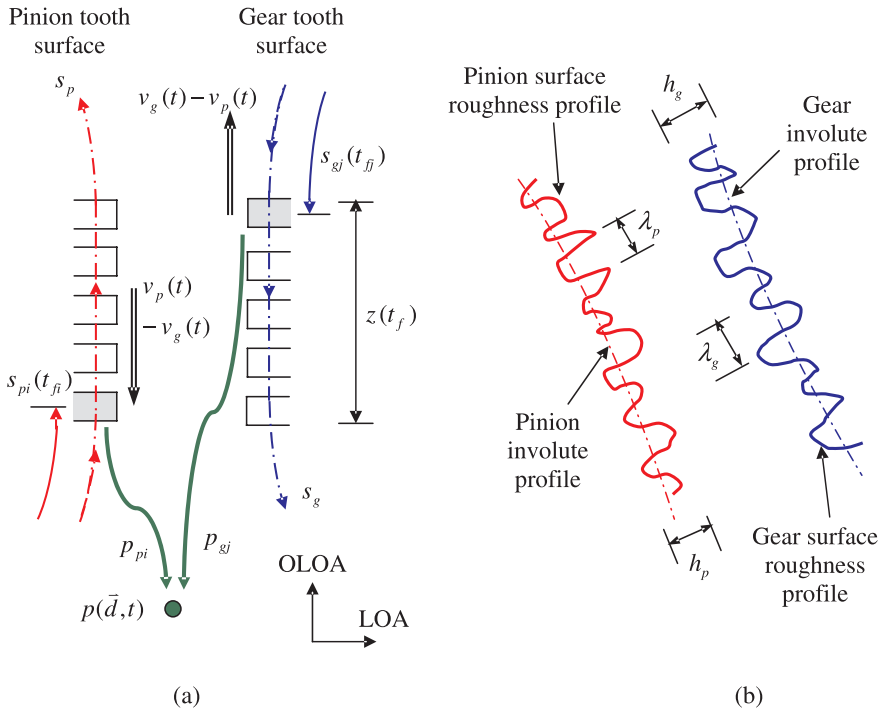

Figure 6. Simplified sound source as generated by the surface roughness. (a) Schematic of sound radiation due to asperity impacts within the gear contact zone; (b) surface roughness description.

Finally, the resulting sound pressures are obtained by superposing the sound pressures from individual asperities of pinion and gear teeth as follows. Here p_{piln} and p_{giln} represent the equation (18) and subscripts l, n denote asperity indices over involute and face width directions respectively. Further, subscripts i and j are tooth indices of pinion and gear respectively.

$$p(d,t) = \sum_i \sum_l \sum_n p_{piln}(t, t_{f,pilm}) + \sum_j \sum_l \sum_n p_{giln}(t, t_{f,gilm}). \tag{28}$$

A numerical example is presented to illustrate the level of sound radiated from the surface asperities on gear teeth. Consider the pinion speed of 1500 rpm with an average asperity height of 1 μm. The asperity beam width and thickness are assumed to be $b = 0.7h$ and $t = 0.7h$ respectively. Key parameters for this gear example are summarized in Table 1. First, the normal forces between meshing gear teeth are calculated along with the contact location and the instantaneous radius of curvature. Then, the width of instantaneous contact zone is obtained by (27) and the calculated $z(t)$ is shown in Figure 7 for one mesh cycle. Figure 7 shows that the first tooth pair departs from contact after approximately 0.7 ms of each mesh cycle. But, the second pair remains in contact during the entire mesh cycle.

Now, the sound pressures at a distance of 1.0 m from the gear contact are calculated at the pinion speed of 1500 rpm and with surface roughness of $h = 1$ μm; this assumes that only

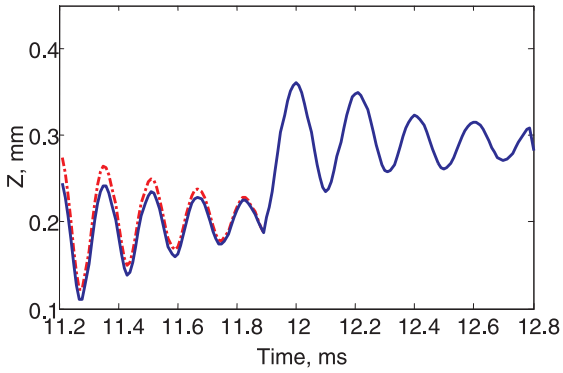

Figure 7. Calculated width of the instantaneous contact zone for the example of Table 1. Key: ——, second pair of teeth; - - - -, first pair of teeth.

Table 1. Parameters of the spur gear system (for one mesh cycle) and asperity dimensions.

Description	Parameter	Dimension/Value
Gear pair	Numbers of teeth	25 (*pinion*) and 31 (*gear*)
	Pinion speed	1500 rpm (baseline)
	Center distance	88.9 mm
	Profile contact ratio	1.433
	Mesh period	1.6 ms
	Gear tooth face width	31.75 mm
Surface roughness	Asperity height (h)	1.0 μm (baseline)
	Average asperity distance	0.6 h +1.0 μm
	Asperity width	0.2 h
	Asperity thickness	0.2 h
	Young's modulus	19.5×10^{10} (Pa)
	Poisson's ratio	0.28
	Density	7700 (kg/m^3)

one surface finish induced air-borne source is present though many structure- and air-borne sources are likely in a real-life geared system. The time histories of sound pressures are shown in Figures 8(a), (b), (c) and (d) respectively for 26 mesh cycles: pinion of the first tooth pair, gear of the first tooth pair, pinion of the second tooth pair and gear of the second tooth pair. Similarly, sound pressure spectra that are radiated from the tooth pair components are shown in Figure 9(a) to (d). Asperities are randomly distributed with a mean distance over the tooth curvature in the involute direction. Hence, each mesh cycle has alternate asperity distributions. Figure 8 shows that the time domain signatures of the radiated sound pressures do not seem to depict a distinctive characteristic. However, it is further observed in Figure 8 that the sound pressures from the first tooth pair exhibit some discontinuities between mesh cycles as expected from the disengagement of the tooth pair during the latter part of mesh cycles unlike the second pair.

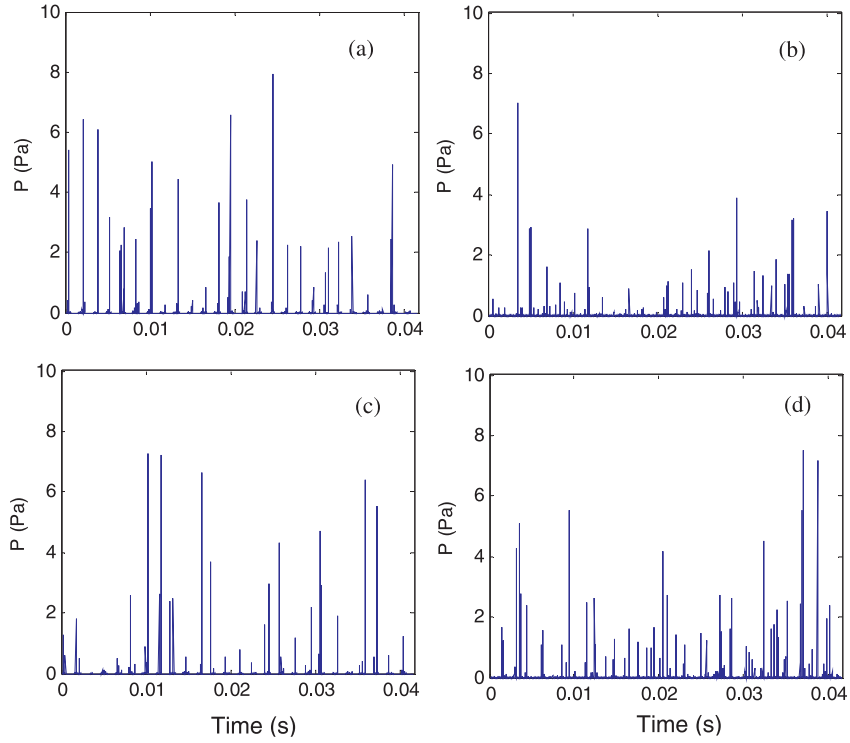

Figure 8. Time histories of the radiated sound pressures at 1500 rpm given surface roughness height of $h = 1$ μm. (a) Sound pressure from pinion of the first tooth pair; (b) gear of the first tooth pair; (c) pinion of the second tooth pair; (d) gear of the second tooth pair.

Next, the effects of operating speeds and surface roughness conditions on the sound pressure spectra (in terms of the gear mesh harmonics) are considered. First, the effect of operating speed on the sound pressures, which are averaged over the mesh harmonics, are shown in Figure 10 given $h = 1$ μm. Observe that the noise is distributed over a broad range of frequencies and no pure tone seems to be evident. Further, the sound increases with the gear operating speed over the entire frequency range, as shown in Figure 10. Next, the effect of surface roughness height (h) is illustrated in Figure 11 at 1500 rpm. Again the sound pressure increases with h over all spectral bands.

Table 2 compares theoretical and experimental spectrally-averaged sound pressure levels on an order of magnitude basis. Note that the measured sound levels from disk-tip experiments were reported by Othman et al. (1990) and they are not from gears in contact. Nevertheless, Table 2 shows that the measured sound pressure levels increase with h; this is what our model predicts though levels are affected by the modal damping ratios as shown in Table 2. Further, gear noise experiments (say at 1500 rpm with 662 to 1875 pounds per inch of tooth load as compiled by Mitchell, 1971), exhibit an increase of about 1.5 dB when h is raised from 1 μm to 2.5 μm (and again by 1.5dB when h is raised to 5 μm). Our prediction shows about 6 to 3 dB increase for the same changes in h. Similarly, another set of experimental data for AGMA quality 11 gear (with an involute profile error of 6–8 $\times$ 10^{-4} inch)

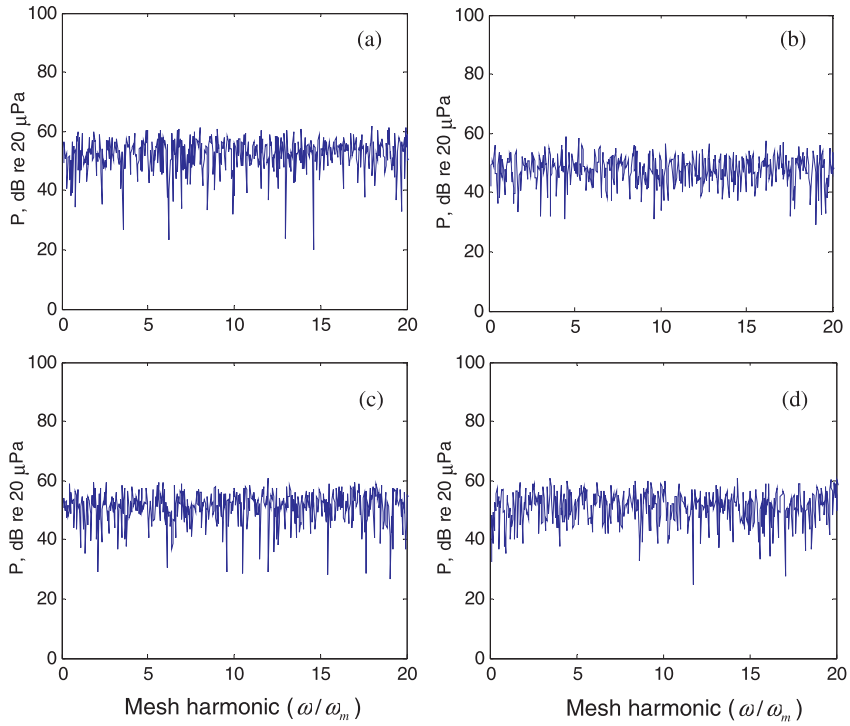

Figure 9. Sound pressure spectra at 1500 rpm given $h = 1$ μm. (a) Sound pressure from pinion of the first tooth pair; (b) gear of the first tooth pair; (c) pinion of the second tooth pair; (d) gear of the second tooth pair.

Table 2. Effect of surface roughness height (h) on the spectrally averaged sound pressure level (SPL in dB re 20 μPa)

Prediction based on our gear dynamics model (at 1500 rpm)	Surface roughness	$h = 2$ μm	$h = 5$ μm	$h = 10$ μm
For 1% modal damping	SPL (dB)	64	67	69
For 5% modal damping	SPL (dB)	59	60	61
Measurement by Othman et al. (1990)on disk-tip experiments (with steel specimen; contact load = 1N)	Surface roughness	$h = 2$ μm	$h = 5$ μm	$h = 10$ μm
	SPL (dB)	48	53	56

yields a slope of approximately 5 dB per octave with respect to speed (from 500 to 4000 rpm) as documented by Mitchell (1971); our model predicts a slope of 8 to10 dB per octave for the same speed range. Though analytical and experimental sound level magnitudes or trends appear to be similar, it should be noted that we have made several simplifying assumptions in our model, and some caution should be exercised in the interpretation of results. For instance, our model predicts only friction-induced airborne noise whereas the measurements reported

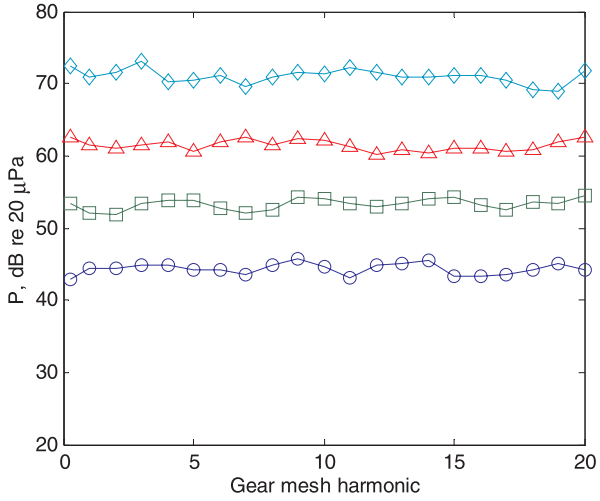

Figure 10. Effect of operating speed on sound pressure spectra given $h = 1$ μm. Key: —○—, 500 rpm; —□—, 1000 rpm, —△—, 2000 rpm, —◇—, 4000 rpm.

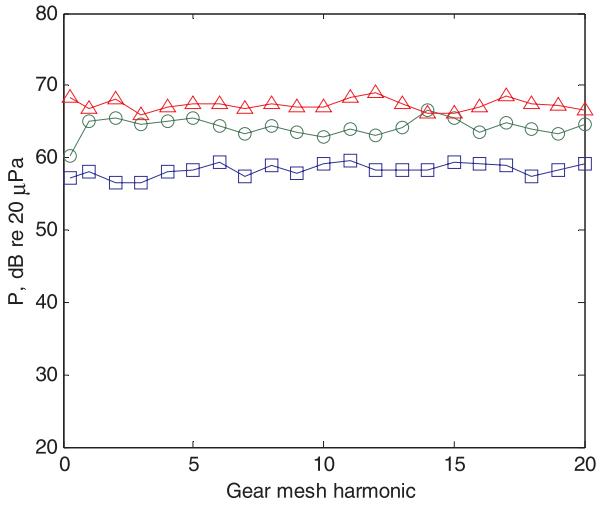

Figure 11. Effect of surface roughness height (h) on sound pressure spectra at 1500 rpm. Key: —□—, $h = 1$ μm; —○—, $h = 2.5$ μm, —△—, $h = 5$ μm.

in the literature include all noise generation mechanisms such as structure-borne noise from surrounding structures and impact-induced noise.

7. CONCLUSIONS

A new analytical formulation for the air-borne noise source as generated by the gear tooth surface roughness has been developed. It describes the source in terms of the sliding contacts between meshing gear teeth. Given the instantaneous sliding velocity between pinion and gear teeth as the initial conditions, the surface asperities on tooth surfaces, which are modeled as compact structural beam elements, radiate sound in the off-line of action after sliding impacts occur against asperities of the meshing part. Sound pressure predictions as yielded by a linear time-varying model of a spur gear pair (with sliding friction) show that the noise level increases with operating speeds and surface roughness parameter (h). Such sound pressure relations with operating speeds and surface roughness appear to match well with some empirical data that have been reported by prior researchers (Mitchell, 1971; Othman et al., 1990; Baranov et al., 1997). Nevertheless, new measurements on gear pairs with known surface roughness parameters must be made over a range of operating conditions including temperature, before quantitative comparisons can be made. Further, relative importance of friction-induced noise needs to be characterized with respect to other gear noise sources such as structure-borne noise due to the dynamic transmission error, tooth impact-induced noise and so on; these are often radiated by the gearbox and surrounding structures. Ideally, one should develop experimental methods to differentiate between different gear noise sources. Further, the interactive effects of sliding friction, lubrication oil properties (over a wide range of operating temperatures) and surface finish on gear noise need to be better understood. Future work should also include an examination of non-periodic and periodic surface undulations.

APPENDIX A: LIST OF SYMBOLS

A, B, C, D	arbitrary constants
B	beam width
$c(t)$	damping coefficient
c	sound wave speed
d	distance to acoustic field point
EI	flexural rigidity of beam
f	force
G	arbitrary function
g	Green's function
h	asperity height
J	mass moment of inertia
k	stiffness
L	beam length
N	normalization function
p	sound pressure
Q	arbitrary function
q	free vibration response of mode
R	radius
s	involute coordinate

T	torque
t	time
v	velocity
x	coordinate in line of action
y	coordinate in off-line of action
z	width of contact zone
α	roll angle
γ	radius of curvature
δ	impact length over asperity beam
Ξ	dynamic transmission error
ε	arbitrary function for mode
κ	wave number
λ	distance between asperities
μ	friction coefficient
ν	Poisson's ratio
θ	rotational displacement
Λ	root of free vibration equation
σ	real part of root of free vibration equation
ρ	mass density
Φ	velocity potential
ψ	gear angle
ϕ	mode
ω	frequency (rad/sec)

Subscripts

b	base circle
c	mesh cycle
d	damped
f	friction
g	gear
i, j	indices of pinion and gear
L	start of mesh cycle of gear
l, n	asperity indices
m	meshing point
N	normal
p	pinion
r	mode index
0	start of mesh cycle of pinion

Superscripts

$\cdot$	time derivative
$*$	complex conjugate

Operators

$\delta[\cdot]$	Dirac delta function
∇	Laplace operator

Acknowledgements. This article is based upon a three-year study that was supported by the US Army Research Laboratory and the US Army Research Office under contract/grant number DAAD19-02-1-0334. This support and the encouragement by Dr G. L. Anderson (project monitor) are gratefully acknowledged. The Rotorcraft Industry Technology Association (RITA) is also thanked for supporting this research.

REFERENCES

Akay, A., 2002, "Acoustics of friction," *The Journal of the Acoustical Society of America* **111**(4), 1525–1548.

Aziz, S. M. A. and Seireg, A. A., 1994, "A parametric study of frictional noise in gears," *Wear* **176**, 25–28.

Baranov, V. M., Kudryavtsev, E. M., and Sarychev, G. A., 1997, "Modeling of the parameters of acoustic emission under sliding friction of solids," *Wear* **202**, 125–133.

Goldsmith, W., 2001, *Impact: The Theory and Physical Behavior of Colliding Solids*, Dover, Mineola, NY.

Houjou, H. and Umezawa, K., 1992. "A generation mechanism of aerodynamic sound of spur gears," in *ASME International Power Transmission and Gearing Conference* DE-**43**(2), Scottsdale, AZ, September 13–16, pp.597–604.

Houser, D., 1991, "Gear noise," in *Dudley's Gear Handbook*, McGraw-Hill, New York, Chapter 14.

Houser, D. and Singh, R., 2001, *Gear Noise Short Course Notes*, The Ohio State University.

Ishida, K. and Matsuda. T., 1980, "Effect of tooth surface roughness on gear noise and gear noise transmitting path," Report ASME 80-C2/DET-70.

Jacobson, M. F., Singh, R., and Oswald, F. B., 1996, "Acoustic radiation efficiency models of a simple gearbox," in *ASME International Power Transmission and Gearing Conference*, DE-88, San Diego, CA, October 6–9, 597–601.

Mark, W. D., 1992, "Contributions to the vibratory excitation of gear systems from periodic undulations on tooth running surfaces," *The Journal of the Acoustical Society of America* **91**(1), 166–186.

Mitchell, L. D., 1971, "Gear noise: the purchaser's and the manufacturer's view," in *Proceedings of the Purdue Noise Control Conference,* West Lafayette, IN, July 14–16, pp.95–106.

Othman, M. O., Elkholy. A. H., and Seireg, A. A., 1990, "Experimental investigation of frictional noise and surface-roughness characteristics," *Experimental Mechanics* **30**, 328–331.

Singh, R. and Kim, S., 2003, "Examination of multi-dimensional vibration isolation measures and their correlation to sound radiation over a broad frequency range," *Journal of Sound and Vibration*, **262**(3), 419–455.

Stepanishen, P. R., 1971, "Transient radiation from pistons in an infinite planar baffle," *The Journal of the Acoustical Society of America* **49**, 1629–1638.

Timoshenko, S, Young, D. H., and Weaver, W., 1974, *Vibration Problems in Engineering,* John Wiley & Sons, Inc, New York.

Vaishya, M. and Singh, R., 2001, "Analysis of periodically varying gear mesh systems with coulomb friction using floquet theory," *Journal of Sound and Vibration* **243**(3), 525–545.

Vaishya, M. and Singh, R., 2003, "Strategies for modeling friction in gear dynamics," *Transactions ASME. Journal of Mechanical Design* **125**, 383–393.